

# ECE540 Project III: Infinitely Long Conducting Cylindrical Scatterer with Various Incident Angles and Geometries Investigated by Moment Method

Yi-Chia Tsai (NetID: yichiat2)<sup>a)</sup>

Department of Electrical and Computer Engineering, University of Illinois at Urbana-Champaign, Urbana, Illinois 61801, USA and Micro and Nanotechnology Laboratory, University of Illinois at Urbana-Champaign, Urbana, Illinois 61801, USA

(Dated: 12 December 2019)

Moment Method (MoM) has been implemented to solve the scalar Helmholtz equations and study the two-dimensional electromagnetic waves scattered by infinitely long conducting cylinders. The impact of different incident angles and scatterer geometries on scattered and total fields are investigated. Technically, TM and TE polarization are considered by solving electric-field (EFIE) and magnetic-field (MFIE) integral equations, where Green's functions and its derivatives are expressed by the zeroth-order and first-order Hankel functions of the second kind, respectively. The results show that the impact of edge singularity and edge diffraction on surface current density have been captured for TM and TE cases. The objectives of this project are to (1) understand how to formulate EFIE and MFIE, (2) assemble individual segments of conducting cylinders into an interacting matrix, (3) solve the matrix to obtain surface current density, and finally (4) calculate the scattered and total fields contributed by the surface current of the conducting cylinders.

Keywords: Moment Method, Scattered field, Total Field, Green's Function, Helmholtz Equation

## I. INTRODUCTION

The scattering of electromagnetic fields (EM-fields) is of great interest in arms and semiconductor industries. In the arms industry, the investigation of scattered field can be used to promote the stealth technology and devise low observable vehicles<sup>1</sup>. On the other hand, in the semiconductor industries, although the device scaling increases the functionality of individual chip and reduces the chip size, the cross-talk of interconnection becomes an important issue because each metal wire radiates and scatters EM-fields in a small dimension. The coupling of EM-fields and source current contributes to noise and is detrimental to the stability and consistency of each chip. Therefore, studying the scattering behavior of conducting materials is necessary.

Common approaches to study EM-fields problems are finite-difference and finite-element methods. The finite-difference method discretizes partial differential equations by mid-point subtractions; whereas, the finite-element method discretizes simulation domains into elements. Therefore, the two methods are general for a wide range of application. However, for open-boundary problems, these two methods have two essential drawbacks: the existence of reflection error and memory-consuming. Although perfectly matched layers are used to absorb the incident wave as much as possible, the reflection still introduces errors to solutions at some levels. On the other hand, large simulation domain is intentionally maintained to study far-field performance. However, the

far-field performance cannot be studied point-by-point, instead, the meshes between observing points and sources need to be solved continuously, meaning that the finite-difference method and the finite-element method cannot study the EM-fields that are too far away from the sources. Additionally, if the simulation domain is too small, the results cannot be recycled for a large domain simulation, implying that simulations need to be completely restarted. Therefore, a better method was developed to for the open-boundary problems: the method of moment (MoM).

MoM is a numerical method to find the sources that contribute to EM-fields directly using the single-source respond function: Green's function. For the scattering of conducting objects, the MoM calculates the surface current density of the conducting objects instead of EM-fields. This means that 3D simulation degenerates into 2D simulation; whereas, 2D simulation degenerates into 1D simulation. This property results in a smaller matrix problem. The far-field, contributed by surface current, at exact points can be calculated individually without the use of large simulation domain. Additionally, if the observing points aren't selected correctly, the EM-fields at arbitrary distance can be re-calculated based on the converged surface current without the need to restart the entire matrix formulation. As a result, the MoM provides tremendous flexibility and efficiency on solving open-boundary problems.

In this project, the scattering of plane waves by infinitely long conducting cylinder is studied, where the scalar Helmholtz equations are discretized using Green's theorems with Green's functions. Since the simulation is 2D, TM and TE modes are considered by solving electric-field (EFIE) and magnetic-field (MFIE) integral equations, respectively. Two different angles that result in the propagation of EM-fields normal to the side of regu-

---

<sup>a)</sup>Address: Innovative COmpound semiconductoR (ICOR) Laboratory, Urbana, Illinois 61801, USA. Electronic mail: yichiat2@illinois.edu. Telephone: +1 (217) 974-5750. URL: <http://icorlab.ece.illinois.edu>.

lar polygons and the propagation of EM-fields parallel to the equiangular line of regular polygons are studied to understand how EM-fields are scattered. Square conducting cylinders with two different sizes ( $1\lambda \times 1\lambda$  and  $3\lambda \times 3\lambda$ ) are studied to understand how EM-fields interacts with large and small conducting objects. Finally, different regular polygons are generated within a  $3\lambda$ -diameter circle to study the shape effect.

## II. COMPUTATIONAL MODEL

### A. TM Formulation: Electric-Field Integral Equations

In the TM mode,  $E_x$  and  $E_y$  are zero. Therefore,  $E_z$  can be obtained by solving scalar Helmholtz equations in frequency domain without solving  $H_x$  and  $H_y$ . First of all, the Helmholtz equations in free space ( $\Omega_\infty$ ) and on the surface of conducting cylinder ( $\Gamma_0$ ) are expressed by

$$\begin{cases} \nabla^2 E_z(\rho) + k_0^2 E_z(\rho) = jk_0 Z_0 J_{i,z}(\rho), & \rho \in \Omega_\infty \\ E_z(\rho) = 0, & \rho \in \Gamma_0 \\ \frac{\partial E_z(\rho)}{\partial n'} = jk_0 Z_0 J_{s,z}(\rho), & \rho \in \Gamma_0, \end{cases} \quad (1)$$

where  $J_{i,z}$  and  $J_{s,z}$  are the current source of incident wave and the induced surface current density; while,  $k_0$  and  $Z_0$  are the wave vector and impedance of free space.  $n'$  is the normal vector of the cylinder surface pointing outward. By applying the second scalar Green's theorem and Huygens' principle,<sup>2</sup> the 2D differential equations of Eq. (1) can be formulated into 1D integral equation:

$$E_z^{inc}(\rho) - jk_0 Z_0 \oint_{\Gamma_0} G_0(\rho, \rho') J_{s,z}(\rho') d\Gamma' = 0, \quad \rho \in \Gamma_0, \quad (2)$$

where  $E^{inc} = e^{jk_0 x}$  is the incident wave propagating toward  $+x$  direction with unity amplitude and  $G_0(\rho, \rho')$  is the Green's function of Helmholtz equation, which can be expressed by the zeroth-order Hankel function of the second kind in 2D system:

$$G_0(\rho, \rho') = \frac{1}{4j} H_0^{(2)}(k_0 |\rho - \rho'|) \quad (3)$$

Notably, Eq. (2) is known as electric-field integral equations (EFIE). The goal of solving Eq. (2) is to procure the induced surface current density ( $J_{s,z}$ ). The far-scattered ( $E_z^{sc}$ ) and total ( $E_z^{tot}$ ) fields can be calculated based on the induced surface current density, expressed by:

$$E_z^{sc}(\rho) = -jk_0 Z_0 \oint_{\Gamma_0} G_0(\rho, \rho') J_{s,z}(\rho') d\Gamma', \quad \rho \in \Omega_\infty \quad (4)$$

$$E_z^{tot}(\rho) = E_z^{inc}(\rho) + E_z^{sc}(\rho), \quad \rho \in \Omega_\infty. \quad (5)$$

### B. TE Formulation: Magnetic-Field Integral Equations

In the TE mode,  $H_x$  and  $H_y$  are zero. Therefore,  $H_z$  can be obtained by solving scalar Helmholtz equations in

frequency domain without solving  $E_x$  and  $E_y$ . First of all, the Helmholtz equations in free space ( $\Omega_\infty$ ) and on the surface of conducting cylinder ( $\Gamma_0$ ) are expressed by

$$\begin{cases} \nabla^2 H_z(\rho) + k_0^2 H_z(\rho) = -[\nabla \times J_i(\rho)]_z, & \rho \in \Omega_\infty \\ H_z(\rho) = -J_{s,t}(\rho), & \rho \in \Gamma_0 \\ \frac{\partial H_z(\rho)}{\partial n'} = 0, & \rho \in \Gamma_0, \end{cases} \quad (6)$$

where  $\nabla \times J_i(\rho)$  and  $J_{s,t}(\rho)$  are the current source of incident wave and the induced surface current density; while,  $k_0$  and  $Z_0$  are the wave vector and impedance of free space.  $n'$  is the normal vector of the cylinder surface pointing outward. By applying the second scalar Green's theorem and Huygens' principle, the 2D differential equations of Eq. (6) can be formulated into 1D integral equation:

$$H_z^{inc}(\rho) - \int_{\Gamma_0} \frac{\partial G_0(\rho, \rho')}{\partial n'} J_{s,z}(\rho') d\Gamma' = -\frac{1}{2} J_{s,t}(\rho), \quad \rho \in \Gamma_0, \quad (7)$$

where  $H^{inc} = e^{jk_0 x}$  is the incident wave propagating toward  $+x$  direction with unity amplitude and  $G_0(\rho, \rho')$  is the Green's function of Helmholtz equation, which is identical to Eq. (3). However, different from the TM mode, the surface magnetic field is not zero, which requires the consideration of  $n'$  in the principle value integral of Eq. (7). As a result, the partial differential of Green's function with respect to the normal vectors of cylinder surface is expressed by the first-order Hankel function of the second kind in 2D system:

$$\frac{\partial G_0(\rho, \rho')}{\partial n'} = \frac{k_0}{4j} H_1^{(2)}(k_0 |\rho - \rho'|) \frac{\hat{n}' \cdot (\rho - \rho')}{|\rho - \rho'|} \quad (8)$$

Notably, Eq. (7) is known as magnetic-field integral equations (MFIE). The goal of solving Eq. (7) is to procure the induced surface current density ( $J_{s,t}$ ). The far-scattered ( $H_z^{sc}$ ) and total ( $H_z^{tot}$ ) fields can be calculated based on the induced surface current density, expressed by:

$$H_z^{sc}(\rho) = \oint_{\Gamma_0} \frac{\partial G_0(\rho, \rho')}{\partial n'} J_{s,z}(\rho') d\Gamma', \quad \rho \in \Omega_\infty \quad (9)$$

$$H_z^{tot}(\rho) = H_z^{inc}(\rho) + H_z^{sc}(\rho), \quad \rho \in \Omega_\infty. \quad (10)$$

### C. Generation of Regular Polygons

Since the impact of different shape of regular polygons on EM-fields is considered, a consistent approach to generate regular polygons is important. Here, a circle with a diameter of  $3\lambda$  centering at  $(0,0)$  is generated and discretized uniformly by 360 points. Next,  $N$  indices are sampled uniformly among the 360 points for a  $N$ -side regular polygon. The  $x$  and  $y$  coordinates of the  $n^{th}$  index are expressed by

$$\begin{cases} x(n) = \cos(n \cdot \frac{360}{N}) \\ y(n) = \sin(n \cdot \frac{360}{N}) \end{cases} \quad n = 1 \dots N \quad (11)$$

The advantage of this approach is that every regular polygons are generated within the same circle, meaning that the shape effect can be isolated. On the contrary, if the side length is fixed as  $3\lambda$ , the volume of regular polygon increases unbounded as  $N$  increases, which is not suitable for the discussion of shape effect.

#### D. Rotation of the Conducting Cylinders

According to Eq. (11), one of the indices of regular polygons will always be on the  $x$ -axis, meaning that the initial orientation of the generated regular polygon is fixed. In this case, the calculated results are not comparable because the incident EM-fields propagating along  $+x$  direction may impact the side perpendicularly in one regular polygon but not for another regular polygon. In order to study the impact of incident angle on EM-fields and unify the incident angle for comparison, two solutions are proposed. The first solution is to change the incident angle of incident EM-fields directly because it will complicate the comparisons and poly-analysis between different regular polygons. The other solution is to rotate the indices of regular polygons through rotational matrix:

$$\begin{bmatrix} \mathbf{x}' \\ \mathbf{y}' \end{bmatrix} = \begin{bmatrix} \cos(\theta) & -\sin(\theta) \\ \sin(\theta) & \cos(\theta) \end{bmatrix} \begin{bmatrix} \mathbf{x} \\ \mathbf{y} \end{bmatrix} \quad (12)$$

where  $\theta$  is the rotation angle defined counterclockwise.

### III. RESULTS AND DISCUSSION

In this section, the discussions are boiled down to 3 subsections: Size Effect, Angle Effect, and Shape Effect, which aim to study the impact of the size of scatterers, the incident angle, and the shape of scatterers on scattered and total fields. Each side is divided into 30 segments for the calculation of surface current density. To study the scattered and total fields, a  $5\lambda \times 5\lambda$  free space is constructed in the following analysis.

#### A. Size Effect

Figs. 1 and 2 show the MoM solutions of plane wave scattered by the  $1\lambda \times 1\lambda$  and  $3\lambda \times 3\lambda$  square conducting cylinders. The propagation direction of the incident wave is perpendicular to one of the side of the scatterer. The left column shows the TM mode; while, the right column shows the TE mode. The magnitude of the surface current densities induced by electric field (TM mode) and magnetic field (TE mode) are shown in Fig. 1(a) and (b) ( $1\lambda \times 1\lambda$  case) and Fig. 2(a) and (b) ( $3\lambda \times 3\lambda$  case), respectively.  $s$  starts from the upper rightmost corner of the square conducting cylinder and increases counterclockwise. The blue lines are predicted by the MoM;

while, the red dashed lines are approximated by the Physical Optics (PO) approximation.<sup>2</sup> Without discussing in the ECE540 lecture, the PO is actually a method to approximate the surface current density of perfect electric conductor (PEC) in a dielectric medium using equivalence principle, which merges two distinct media into one medium with equivalent current densities. In the PO approximation, the reflected fields are identical to the incident fields, therefore, the surface current densities can be expressed as

$$\mathbf{J}_s = \hat{\mathbf{n}} \times (\mathbf{H}_i^{inc} + \mathbf{H}_i^{ref}) \approx \hat{\mathbf{n}} \times 2\mathbf{H}_i^{inc} \approx \mathbf{J}_s^{PO}, \quad (13)$$

where  $\hat{\mathbf{n}}$ ,  $\mathbf{H}^{inc}$ , and  $\mathbf{H}^{ref}$  are the normal vector of PEC-dielectric interface, the incident and reflected magnetic fields, respectively. Thus, the MoM results are quite consistent with the PO approximation on the side that scatters the incident wave. However, the PO approximation is valid only for the infinitely large PEC-dielectric interface. The finite size of the scatterer gives rise to the smooth decay of surface current densities on the other sides. Due to the finite size of the scatterer, the PO approximation also cannot capture the edge effect. Contrarily, the MoM results in the TM mode successfully retain the edge singularity, contributing to 4 sharp peaks on Fig. 1(a) and 2 sharp peaks on Fig. 2(a). Fig. 2(a) has less sharp peaks for two reasons: (1) the side length of scatterer is larger than the wavelength and (2) the scattered field at the opposite side of the scatterer is much weaker, which will be discussed later. On the other hand, the interference pattern of surface current densities is captured by the MoM in the TE mode, but not by the PO approximation. This is, again, because the PO approximation fails to include the edge effect, but the MoM results recovers the edge diffraction. As a result, one and three peaks are observed in the front side of Fig. 1(b) and Fig. 2(b), respectively.

Fig. 1(c) and (e) show the scattered and total fields of the  $1\lambda \times 1\lambda$  scatterer in the TM mode; while, the Fig. 1(d) and (f) show the corresponding properties in the TE mode, respectively. On the other hand, for the comparison, Fig. 2(c) and (e) plot the scattered and total fields of the  $3\lambda \times 3\lambda$  scatterer in the TM mode; while, the Fig. 2(d) and (f) show the corresponding properties in the TE mode, respectively. As shown in the scattered fields, two peaks are observed, which are in the front and back sides of the scatterer. According to the surface equivalence principle<sup>3</sup>, the scattered field in the front side is radiated by the induced surface current; while, the scattered field in the back side is induced by the surface magnetic current, which is similar to Eq. (13) and can be approximated by the induction theorem (IT)<sup>2</sup>:

$$\mathbf{M}_s = \hat{\mathbf{n}} \times (\mathbf{E}_i^{inc} + \mathbf{E}_i^{ref}) \approx \hat{\mathbf{n}} \times 2\mathbf{E}_i^{inc} \approx \mathbf{M}_s^{IT}, \quad (14)$$

Consequently, the scattered fields in the front side are known as the reflected fields, which couple with the incident fields and lead to the intense total fields in the front side. On the contrary, the scattered fields in the back

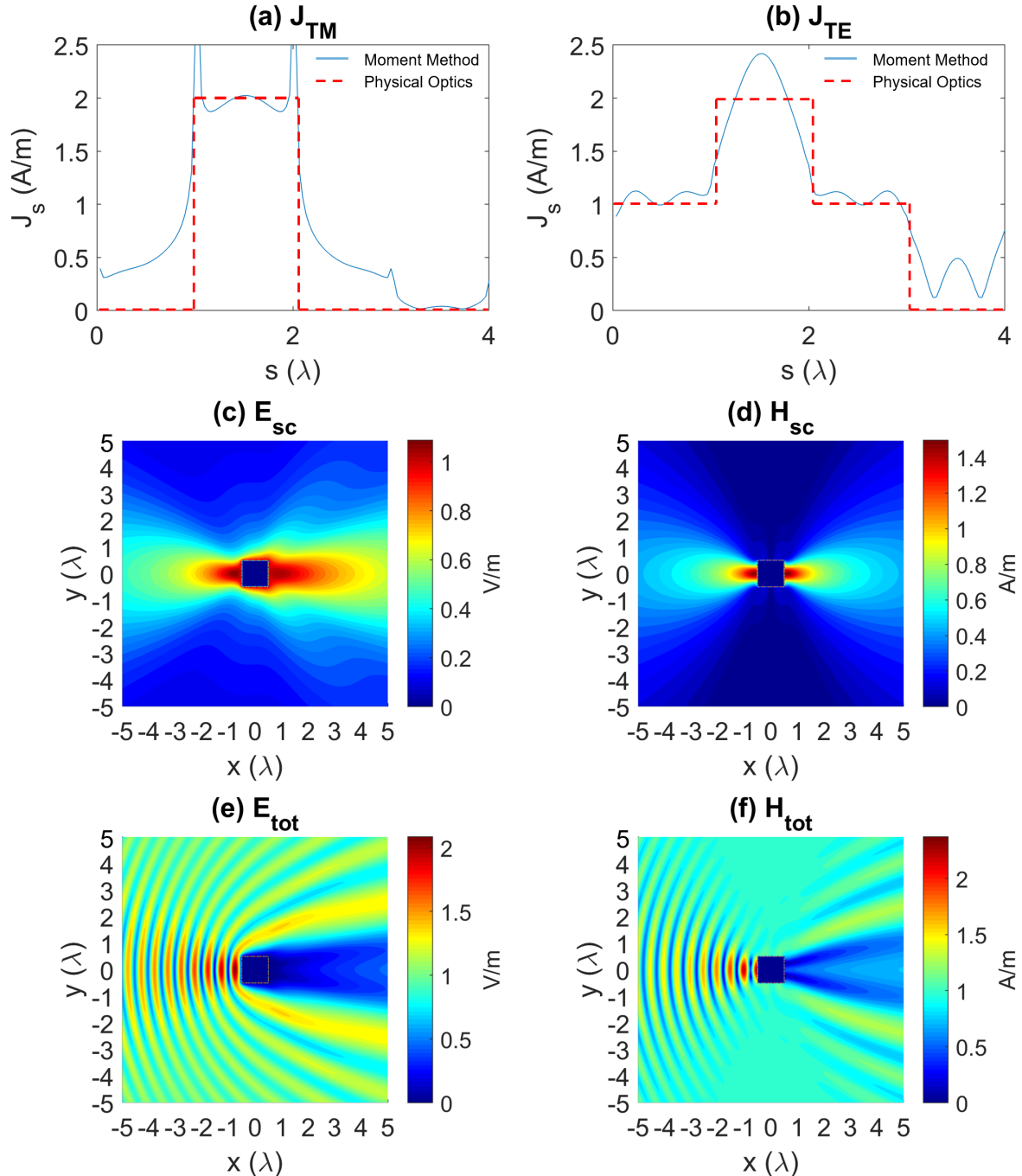


**FIG. 1** The scatterer is a  $1\lambda \times 1\lambda$  square conducting cylinder, where the propagation direction of the incident wave is perpendicular to one of the side of the scatterer. The left column shows the TM mode; while, the right column shows the TE mode. Magnitude of the induced surface current density in the (a) TM and (b) TE modes.  $s$  starts from the upper rightmost corner. Magnitude of the scattered field in the (c) TM and (d) TE modes. Magnitude of the total field in the (e) TM and (f) TE modes.

side have an opposite phase, canceling the incident fields and leading to  $\approx 0$  in the total fields. The major differ-

ence between TM and TE modes is that the distribution of surface current densities is influenced by the interfe-

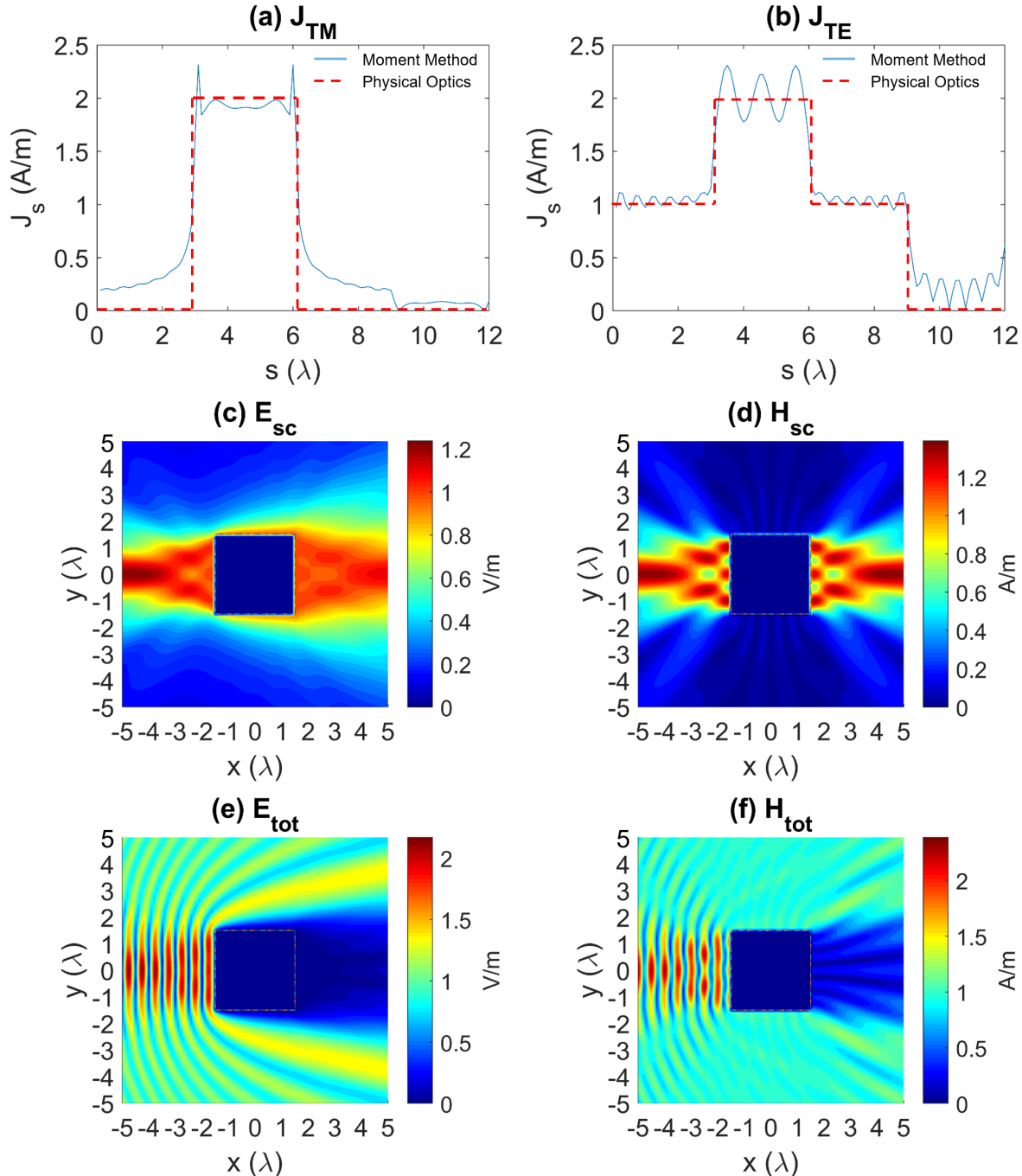


**FIG. 2** The scatterer is a  $3\lambda \times 3\lambda$  square conducting cylinder, where the propagation direction of the incident wave is perpendicular to one of the side of the scatterer. The left column shows the TM mode; while, the right column shows the TE mode. Magnitude of the induced surface current density in the (a) TM and (b) TE modes.  $s$  starts from the upper rightmost corner. Magnitude of the scattered field in the (c) TM and (d) TE modes. Magnitude of the total field in the (e) TM and (f) TE modes.

ence of surface waves excited by the edge diffraction. As a result, the interference pattern can be observed in the

scattered and total fields of the TE mode, as shown in Fig. 1(d)-(f) and Fig. 2(d)-(f).

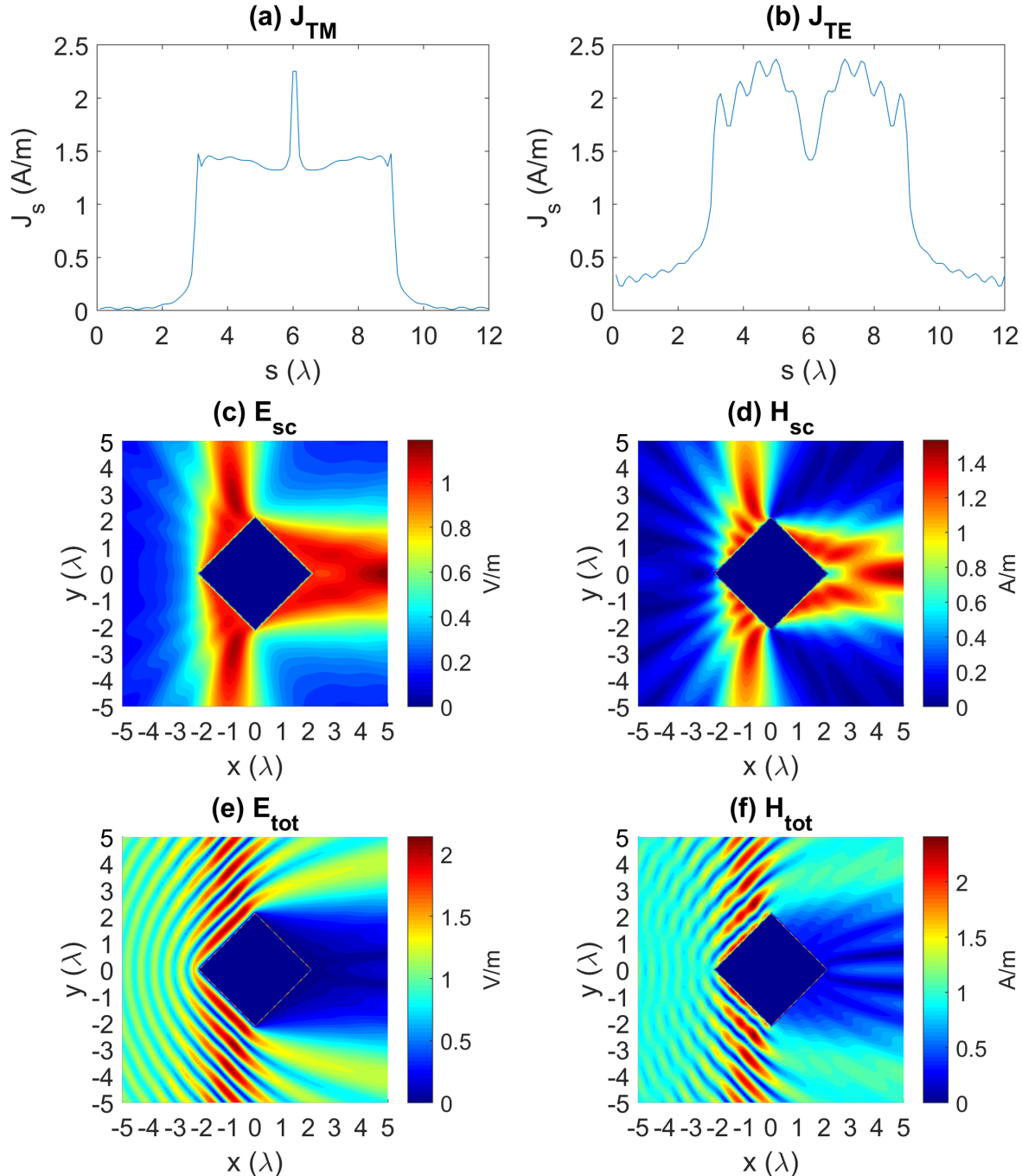


**FIG. 3** The scatterer is a  $3\lambda \times 3\lambda$  square conducting cylinder rotating with 45 degrees, where the propagation direction of the incident wave is parallel to one of the equiangular lines. The left column shows the TM mode; while, the right column shows the TE mode. Magnitude of the induced surface current density in the (a) TM and (b) TE modes.  $s$  starts from the upper corner. Magnitude of the scattered field in the (c) TM and (d) TE modes. Magnitude of the total field in the (e) TM and (f) TE modes.

Finally, the major difference between Fig. 1 and Fig. 2 is that the longer side length of  $3\lambda \times 3\lambda$  scatterer allows

more edge diffraction modes, resulting in more significant interference patterns on the scattered and total fields.

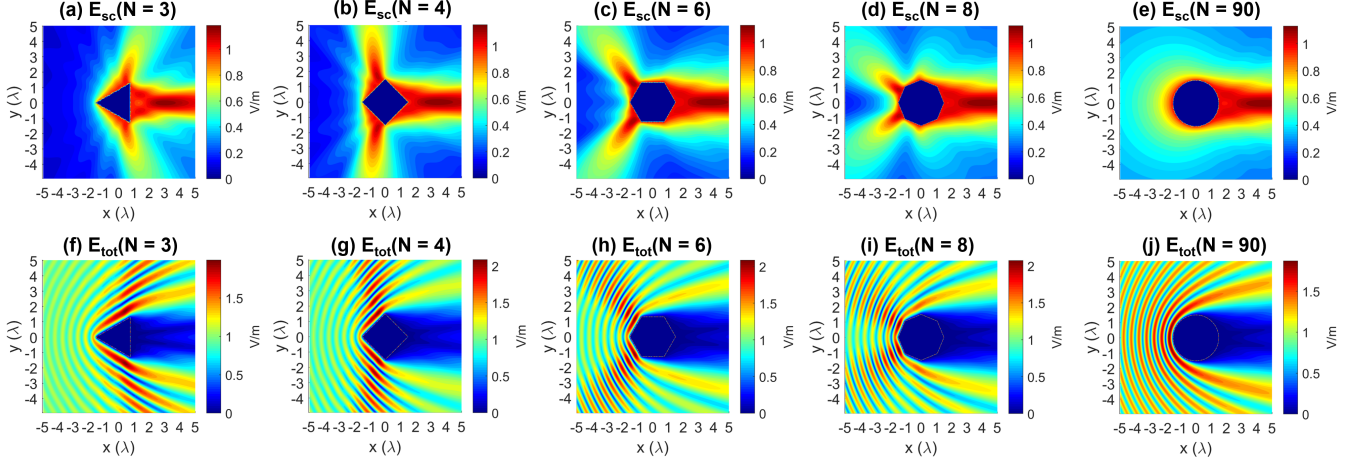


**FIG. 4** The scattered (upper figures) and total (lower figures) fields of regular polygons with  $N = 3, 4, 6, 8$ , and 90 in the TM mode. The regular polygons are rotated so that the propagation direction of the incident wave is parallel to one of the equiangular lines.

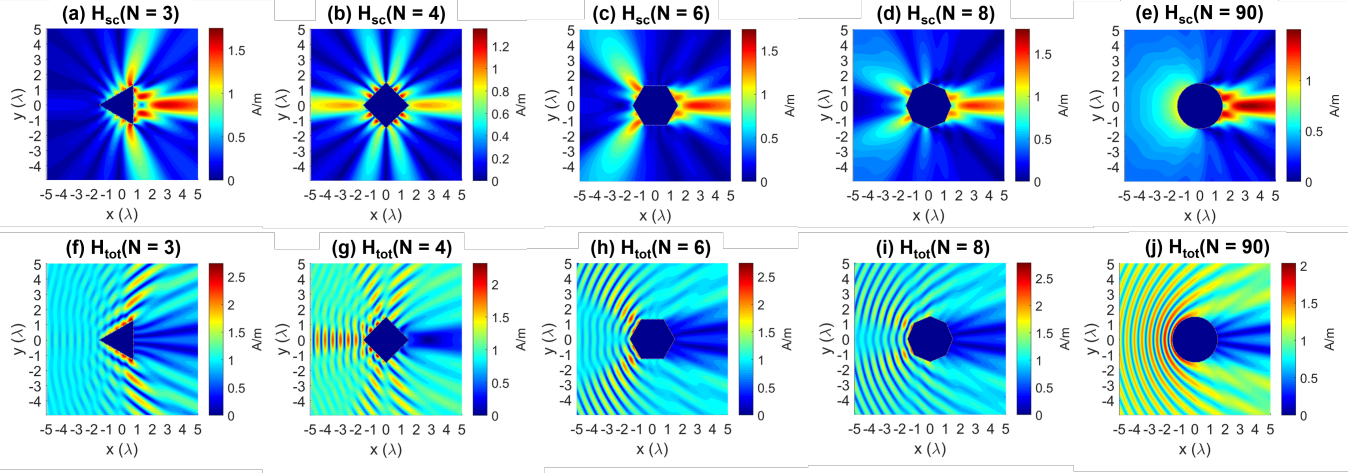


**FIG. 5** The scattered (upper figures) and total (lower figures) fields of regular polygons with  $N = 3, 4, 6, 8$ , and 90 in the TE mode. The regular polygons are rotated so that the propagation direction of the incident wave is parallel to one of the equiangular lines.

## B. Angle Effect

So far, the EM-fields scattered by square conducting cylinders have been procured by the MoM and analyzed together with PO and induction theorem. However, the approximation that the reflected field is identical to the incident field is valid only when the incident wave is normal the surface of PEC-dielectric interface and the interface is infinitely long. In the previous section, the impact of finite edge has been scrutinized. In this part, different incident angle is considered.

Fig. 3 the MoM solutions of plane wave scattered by the  $3\lambda \times 3\lambda$  square conducting cylinders rotating with 45 degree. The propagation direction of the incident wave is parallel to one of the equiangular lines of the scatterer. The left column shows the TM mode; while, the right column shows the TE mode. The magnitude of the surface current densities induced by electric field (TM mode)

and magnetic field (TE mode) are shown in Fig. 3(a) and (b), respectively.  $s$  starts from the upper corner of the square conducting cylinder and increases counterclockwise. First of all, the induced surface current densities are more concentrated in the front sides, which have two sides compared to one in Fig. 2). According to the surface equivalent principle, the induced surface current densities in the front sides radiate and contribute to the scattered fields. The direction of the scattered fields in the front sides are perpendicular to the incident EM-fields because the incident angle is 45 degrees, which is identical to the reflected angle of 45 degrees. On the contrary, the scattered fields in the back sides are radiated by the surface magnetic current according to the induction theorem. As a result, the scattered fields in the front sides couple with the incident fields and strengthen the total fields along the direction normal to the incident fields; while, the incident fields in the back sizes are cancelled by the scattered

fields, leading to the total fields of  $\approx 0$  for both TM and TE modes. By comparing Fig. 2 and Fig. 3, the major difference is that the reflection of EM-fields are significantly dependent on the incident angle. On the other hand, the scattered and total fields on the opposite sides of the scatterer have the similar distribution, but the influenced region is dominant by the side length of  $3\lambda$  in Fig. 2 and the diagonal of  $3\sqrt{2}\lambda$  in Fig. 3.

### C. Shape Effect

In this section, the impact of imperfect circular conducting scatterers on the scattered and total fields are investigated. Regular polygons with different number of sides are adopted to emulate the imperfection. As introduced in Section II C, different regular polygons are generated in the same circle with  $3\lambda$  diameters, thus the side length ( $l$ ) is defined by

$$l = 3\lambda \cdot \sin\left(\frac{180}{N}\right) \quad (15)$$

where  $N$  denotes the total number of sides in the regular polygons.

Fig. 4 illustrates the MoM solutions of plane wave scattered by the regular polygons with  $N = 3$  (triangle), 4 (square), 6 (hexagon), 8 (octagon), and 90 ( $\approx$  circle) in the TM mode, where the regular polygons are rotated by 60, 45, 30, 22.5, and 2 degrees, respectively, so that the propagation direction of the incident wave is in alignment with one of the equiangular lines of the regular polygons. The upper figures show the scattered fields; while, the lower figures illustrate the total fields. First of all, the incident angle becomes smaller with respect to the increased  $N$ , therefore, the induced surface current densities are highly concentrated in the second and third quadrants of the regular polygons. Similar to the previous discussion, the surface current densities contribute to the scattered fields in the front sides, known as the reflected fields. However, what's different from Fig. 3 is that the reflected fields are increasingly intensive along the propagation direction of the incident wave when  $N$  goes larger. This is because the incident angle and reflected angle are smaller when  $N$  increases. As  $N > 4$ , the angle between the incident fields and the reflected fields are smaller than 90 degrees, meaning that the fields are reflected back to the incident direction. The reflected fields couple with the incident fields, leading to the stronger total fields, especially along the incident direction ( $\hat{x}$ ) when  $N$  increases. On the contrary, the scattered fields induced by the surface magnetic current densities in the back sides cancel the incident fields resulting in the  $\approx 0$  total fields in the back sides. The scattered and total fields are uniform and the peak amplitudes decrease because the impact of edge singularity becomes infinitesimal.

Fig. 5 illustrates the MoM solutions of plane wave scattered by the regular polygons with  $N = 3$  (triangle), 4 (square), 6 (hexagon), 8 (octagon), and 90 ( $\approx$  circle) in

the TE mode, where the regular polygons are rotated by 60, 45, 30, 22.5, and 2 degrees, respectively, so that the propagation direction of the incident wave is in alignment with one of the equiangular lines of the regular polygons. The upper figures show the scattered fields; while, the lower figures illustrate the total fields. Similar to the TM mode, the scattered fields in the front sides are strongly dependent on the normal vector of the sides of the incidence, which are a function of  $N$ . In other words, larger  $N$  leads to the smaller angle between the incident wave and the reflected wave. However, in addition to the reflected angle, strong scattered fields are observed on the edges and angles of the regular polygons, especially when  $N$  is smaller than 6. This is because, according to Eq. (15), smaller  $N$  leads to a longer side length, which is able to sustain the edge diffraction, leading to stronger interference. When  $N < 6$ , the side length is longer than the twice of the wavelength, therefore, two interference peaks can be maintained on each side of the scatterer. Yet, when  $N \geq 6$ , the side length is shorter than  $2\lambda$ . Consequently, only one peak exists on each side of the scatterer. Finally, when  $N = 90$ , the scattered fields in the front sides do not have significant peaks and the maximum amplitude decreases because the edge diffraction disappears.

### IV. CONCLUSIONS

In conclusion, the MoM has been implemented to solve scalar Helmholtz equations, which can be boiled down into the EFIE and MFIE equations for TM and TE modes. The plane waves scattered by the conducting cylinders with different sizes, incident angles, and geometries are investigated. In the size effect, I have found that the MoM solutions can capture the edge singularity in the TM mode and the edge diffraction in the TE mode. The large-size scatterer has a stronger interference in the TE mode because of the impact of edge diffraction on the induced surface current densities. In the angle effect, two incident angles are discussed: one is that the propagation direction of incident wave is perpendicular to one of the sides of the scatterer, the other is that the propagation direction of incident wave is parallel to one of the equiangular lines of the scatterer. I found that the scattered fields are parallel to the incident direction in the former case, but are perpendicular to the incident direction (at 90 degrees) in the later case because the incident and reflected angles are the same as 45 degrees. Finally, the shape effect is studied. I found that the scattered and total fields scattered by the regular polygons are strongly dependent on the geometries. For the TM mode, the direction of the scattered fields are changed with respect to  $N$  because large  $N$  renders smaller incident angle and reflected angle. As a result, the total fields are intensified near the incident direction for the large  $N$ ; while, the total fields are intensified at the direction normal to the incident direction for the

small  $N$ . For the TE mode, the trends are similar to the TM mode, however, the edges and angles of the regular polygons generate interference patterns because of the edge diffraction produced by the creeping surface wave traveling around the scatterer.

## ACKNOWLEDGEMENT

This work is supported by the National Science Foundation Faculty Early Career Development (CAREER) Program under award number NSF-ECCS-16-52871. The authors acknowledge the computational resources allocated by Extreme Science and Engineering Discovery Environment (XSEDE) with No. TG-DMR180050

and TG-DMR180075.

<sup>1</sup>Lei Zhu, Xiaolong Liang, Jiong Li, and Rui Li, in *2016 IEEE Advanced Information Management, Communicates, Electronic and Automation Control Conference (IMCEC)* (2016) pp. 1774–1778.

<sup>2</sup>“Electromagnetic theorems and principles,” in *Theory and Computation of Electromagnetic Fields* (John Wiley & Sons, Ltd, 2010) Chap. 3, pp. 73–106, <https://onlinelibrary.wiley.com/doi/pdf/10.1002/9780470874257.ch3>.

<sup>3</sup>S. A. Schelkunoff, *The Bell System Technical Journal* **15**, 92 (1936).

## Appendix A: Source Code Implemented in MATLAB R2019a